ACS APPLIED MATERIALS & INTERFACES
Research Article
www.acsami.org

Polypyrrole-Decorated Ag-TiO_2 Nanofibers Exhibiting Enhanced Photocatalytic Activity under Visible-Light Illumination

Yucheng Yang, Junwei Wen, Jianhong Wei,* Rui Xiong, Jing Shi, and Chunxu Pan*

Key Laboratory of Artificial Micro- and Nano-structures of Ministry of Education and School of Physics and Technology, Wuhan University, Wuhan 430072, People's Republic of China

Supporting Information

ABSTRACT: In this work, a novel photocatalyst, polypyrrole (PPy)-decorated Ag-TiO_2 nanofibers (PPy-Ag-TiO_2) with core−shell structure, was successfully synthesized using an electrospinning technique, followed by a surfactant-directed in situ chemical polymerization method. The results show that a PPy layer was formed on the surface of Ag-TiO_2 nanofiber, which is beneficial for protecting Ag nanoparticles from being oxidized. Meanwhile, the PPy-Ag-TiO_2 system exhibits remarkable light absorption in the visible region and high photocurrent. Among them, the 1%-PPy-Ag-TiO_2 sample shows the highest photoactivity, which is far exceeds that of the single- and two-component systems. This result may be due to the synergistic effect of Ag, PPy, and TiO_2 nanostructures in the ternary system.

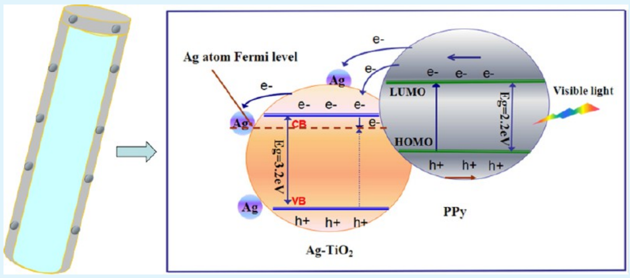

KEYWORDS: *TiO_2-based nanocomposites, silver, conducting polymer, nanofibers, core−shell structures, photocatalysis*

1. INTRODUCTION

Since the discovery of carbon nanotubes,[1] one-dimensional (1D) nanomaterials have been considered as attractive candidates for device applications, because of their dimensional confinement and structurally well-defined physical and chemical properties. TiO_2 nanofibers or nanotubes had attracted much attention for their potential application in the field of pollutant degradation and solar energy conversion, including dye-sensitized solar cells, photocatalyst, and hydrogen energy business.[2−9] However, its wide band gap (3.2 eV) and the low quantum yield largely limited the overall photocatalytic efficiency. To extend the photo response of TiO_2 to the visible region, much effort was made by doping with metal or nonmetal ions, sensitization with organic dyes, conducting polymer, or functional carbonaceous materials,[10−15] etc. Especially, many reports have shown that TiO_2 surfaces modified with conducting polymers such as polyaniline, polypyrrole, polythiophene, and their derivatives can greatly enhance photocatalytic activity for the degradation of organic compounds under visible-light irradiation.[16−22] Our group has also reported that a PANI-sensitized TiO_2 photocatalyst exhibited good photocatalytic activity.[23] Coupling TiO_2 with a conducting polymer can efficiently promote photoinduced electron−hole pair separation in heterojunction photoreciprocal transfer of electrons or holes, thus improving its photocatalytic activity.[24,25]

Meanwhile, how to solve the problem of considerable recombination of the photogenerated electron−hole pairs is another challenge in enhancing the photocatalytic activity. Noble metals have been proven to be good materials for inhibiting electron−hole pair recombination by (1) increasing charge separation within the semiconductor particle, (2) discharging photogenerated electrons across the interface, and (3) providing a redox pathway with low overpotential.[26] Among these noble metals, silver is a popular choice, because of its relatively inexpensive cost, antibacterial property, high work function, and ability to generate surface plasmons at the desired wavelength.[27] However, small silver nanoparticles are very reactive and are easily oxidized and lost. It is therefore beneficial to have a core/shell structure to protect the Ag nanoparticles from being oxidized.

The newly emerging nanotechnology offers another effective solution to improve the photocatalytic activity of TiO_2.[28−30] Choi et al.[31] pointed out that TiO_2 nanofibers have a far more efficient charge separation/transfer process and/or recombination inhibition mechanism than TiO_2 nanoparticles. The main reason is that TiO_2 nanoparticles are three-dimensionally interconnected in TiO_2 nanofibers. A very fast vectorial transport of photogenerated charge carriers (electrons and holes) between the particles may occur in the grain boundaries, resulting in a high photocurrent and photodegradation efficiency. What is more, TiO_2 nanofibers are very hard and strong and thus can maintain its high activity in a variety of conditions, even for long light irradiation periods. Although TiO_2 nanoparticles also have mesopores, they can easily aggregate in their loose and random states, which lower their photocatalytical efficiency.

Received: March 31, 2013
Accepted: June 17, 2013
Published: June 17, 2013

dx.doi.org/10.1021/am401167y | *ACS Appl. Mater. Interfaces* 2013, 5, 6201−6207

Based on the aforementioned considerations, constructing an artificial multicomponent photocatalytical system composed of TiO_2, conducting polymer, and Ag with nanofiber structure is a good strategy for narrowing the band gap and increasing the quantum yield of TiO_2, thereby resulting in enhanced photocatalytic activity.

In this work, we describe an efficient way to synthesis of PPy-decorated Ag-TiO_2 nanofibers (PPy-Ag-TiO_2) with core/shell structure. Although PPy-Ag-TiO_2 thin films have been reported,[32] studies on PPy-Ag-TiO_2 nanofibers are limited. Compared with the corresponding single- and two-component samples, the three-component PPy-Ag-TiO_2 system exhibits enhanced photocatalytic activity in the decomposition of gaseous acetone under visible-light irradiation, which may be due to their high visible-light-gathering ability, fast charge-transfer rate, and low electron−hole recombination based on the photosynergistic effect of TiO_2, Ag, and PPy in the PPy-Ag-TiO_2 system. Moreover, the PPy-Ag-TiO_2 nanofibers can easily be recycled without decreasing the photocatalytic activity because of the large length-to-diameter ratio of the one-dimensional nanostructure.

2. EXPERIMENTAL SECTION

2.1. Electrospinning of Ag-TiO_2 Heterostructure Nanofibers. Ag-TiO_2 heterostructure nanofibers were prepared according to ref 33, with a slight modification. In a typical procedure, 1 g of tetrabutyl titanate (TBT) was dissolved into a mixture, which is composed of 40 mL ethanol and 10 mL acetic acid. After the mixture was stirring for 1h, 4 g of polyvinylpyrrolidone (PVP) was slowly added into the solution. The aforementioned solution was then mixed with a silver nitrate solution (containing 0.1 M $AgNO_3$ and 0.1 M sodium bis (2-ethylhexyl) sulfosuccinate (AOT)/cyclohexane, the mole ratio of $AgNO_3$ to Ti $(OC_4H_9)_4$ was 5%). The solutions were homogeneously stirred for 10 min, and the reducing agent (containing 0.2 M $NaBH_4$ and 0.1 M AOT/cyclohexane) was then added dropwise to the above solution still with continuous stirring. In a typical procedure for electrospinning, the precursor solution was ejected from the plastic syringe (stainless steel needle with 0.4 mm inner diameter). The metallic needle was connected to a high-voltage power supply, and a piece of aluminum foil was placed 10.0 cm below the tip of the needle to collect the nanofibers. The voltage was varied between 10.0 kV and 12.0 kV, and the feeding rate was 1 mL/h. The as-spun nanofibers were then calcined at 500 °C for 3 h in air before cooling to room temperature. Pure TiO_2 nanofibers were similarly prepared but without the addition of $AgNO_3$ solution and the reducing agent. The electrospinning setup consists of three major components: a high-voltage power supply (5−30 kV), a spinneret (a metallic needle), and a collector (a ground conductor). The photograph and schematic of the experimental setup for electrospinning can be found in Figures S1 and S2 in the Supporting Information.

2.2. Preparation of PPy-Decorated Ag-TiO_2 nanofiber. Pyrrole (Aldrich) was distilled in a vacuum prior to use and was immediately used or was refrigerated in air in darkness. In a typical experiment, the obtained Ag-TiO_2 nanofibers were redispersed in a solution containing pyrrole (1.5 mL, 5 mM) and surfactant sodium dodecyl sulfonate (SDS: 0.2 mL, 40 mM) fitted with ultrasonic vibration. SDS can prevent Ag-TiO_2 nanofiber aggregation when pyrrole is oxidized and undergoes seeded polymerization. After 15 min, $FeCl_3{\cdot}6H_2O$ (1.5 mL, 5 mM) aqueous solution was added to the mixture, and ultrasonic vibration was continued for another 0.5 h. The reaction mixture was then incubated at room temperature for 12 h to ensure complete reaction. Finally, the precipitate was centrifuged, washed with deionized water and ethanol several times, and then dried under vacuum at 80 °C until a constant mass was reached. The PPy doping concentration (X) was changed from 0.5 wt % to 2.0 wt %, and the corresponding photocatalysts were called X%-PPy-Ag-TiO_2. For comparison, PPy-TiO_2 nanofibers were prepared under similar conditions. In the study, the content of PPy in PPy-TiO_2 and PPy-Ag-TiO_2 was 1%, unless otherwise stated.

2.3. Characterization. The phases of the samples were characterized by X-ray diffraction (XRD), employing a scanning rate of 0.05° per second in a 2θ ranging from 10° to 80°, using a Bruker D8 Advance X-ray diffractometer (Cu Kα radiation, $\lambda = 1.54178$ Å). The FT-IR spectra of samples were recorded with a Shimadzu IR Prestige-21. The morphologies of the samples were studied by a Shimadzu SSX-550 field-emission scanning electron microscopy (SEM) system, and a JEOL JEM-2010 transmission electron microscopy (TEM). Selected area electron diffraction (SAED) pattern was used to determine the composition of the samples. The UV−vis DRS was performed at room temperature on VARIAN Cary-5000 from 200 nm to 800 nm, using $BaSO_4$ as the reflectance standard. The photoluminescence (PL) spectra were recorded by F-4600 fluorescence spectrophotometer (Hitachi, Japan) under ambient conditions. The excitation wavelength was 315 nm, the scanning speed was 1200 nm/min, and the slot widths of the excitation slit and the emission slit were both 5.0 nm.

2.4. Photoelectrochemical Measurements. The photocurrent developed by irradiating the photoanode (TiO_2) with either UV or visible light was recorded with an electrochemical workstation (Model CHI660A, CH Instruments Co.). The photoelectrochemical cell was a three-electrode system: a TiO_2 film located in the middle of the cell as a working electrode, a saturated calomel electrode as reference, and a platinum wire parallel to the working electrode as a counter electrode. The photoanode was exposed to visible light to measure both open-circuit, photovoltage, and closed-circuit photocurrent. The light source was a 160-W high-pressure mercury lamp with a UV cutoff filter (>420 nm). All measurements were conducted at room temperature and ion a N_2 atmosphere to obtain highly reproducible data. The electrolyte was 0.5 mol/L Na_2SO_4 aqueous solution. The working electrode was activated in the electrolyte for 2 h before measurement. The working electrode potentials were located at 0 V to simulate the same working condition as that of the photocatalysis reaction system.

2.5. Evaluation of Photocatalytic Activity. Gaseous acetone was used as target substrates for the photocatalytic activity test. The photodegradation experiments were carried out in a 8-L reactor under ambient conditions, where a 125-W high-pressure mercury lamp with a 400-nm cutoff filter was used as a visible-light source. Photocatalyst powder (0.5 g) was used for each experiment. Prior to photoreaction, the experiment was carried out in darkness for 2 h to establish adsorption−desorption equilibrium. The concentrations of acetone, carbon dioxide, and water vapor were determined using a gas chromatograph. The photocatalytic activity of the samples was quantitatively evaluated according to the equation

$$\ln\left(\frac{C_0}{C}\right) = kt$$

Here, C_0 and C represent the initial equilibrium concentration and reaction concentration of acetone, respectively; k represents the apparent reaction rate constant, and t represents reactive time.

3. RESULTS AND DISCUSSION

Figure 1 shows the XRD patterns of the different samples. As shown in curve a, the weak reflection centered at $2\theta = 24°$ was characteristic of the doped PPy.[34] The structure of the as-prepared TiO_2 nanofibers was compared with the Joint Committee for Powder Diffraction Standards (JCPDS) data for TiO_2 (File Card No. 21-1272) and was found to be in anatase form (curve b). A comparison of curves c and d in Figure 1 illustrated that the Ag-TiO_2 and PPy-Ag-TiO_2 had similar patterns; both anatase and metallic silver phases (JCPDS File Card No. 89-3722) were detected in their patterns. However, the relative intensity of the TiO_2 and Ag phases decreased in PPy-Ag-TiO_2, indicating their encapsulation by PPy. FT-IR measurement results further confirmed the

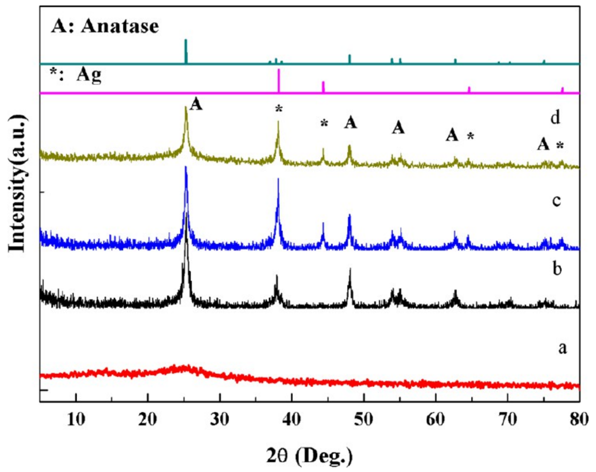

Figure 1. XRD patterns of (a) PPy, (b) TiO_2, (c) Ag-TiO_2, and (d) PPy-Ag-TiO_2.

existence of PPy in the composite. (See Figure S3 in the Supporting Information and the corresponding analysis.)

The controlled morphology of the as-prepared TiO_2 and Ag-TiO_2 nanofibers are shown in Figure 2. Figure 2a presents the typical SEM images of the TiO_2 nanofibers. The diameters of the TiO_2 nanofibers are ~50−200 nm, and the length of the fibers reached a few millimeters. As shown in a TEM image of the TiO_2 nanofibers (Figure 2b), a single nanofiber was composed of many nanoparticles, which agglomerated to form TiO_2 nanofibers during the electrospinning process.[28] The TiO_2 nanocrystals were found to be in anatase form, according to the selected-area electron diffraction (SAED) pattern (inset of Figure 2b); thus, it should be pure TiO_2. The black dots in the TiO_2 nanofibers may be due to the fact that the orientation of the particles was close to Bragg's condition. Consequently, their diffraction was stronger than their transmission, which, in turn, resulted in a darker diffraction contrast image. The Ag-TiO_2 nanofibers (Figure 2c) had a similar size and length with TiO_2 nanofibers but only with some small dots sticking onto the surface (Figure 2d). This similarity was likely due to the use of the same precursor and synthesis route only in the presence of $AgNO_3$ solution. According to a typical TEM image of Ag-TiO_2 nanofibers (Figure S4 in the Supporting Information), the average size of a silver particle was determined to be 18.02 nm (see Figure S5 in the Supporting Information).

The controlled morphology of the as-prepared PPy-TiO_2 and PPy-Ag-TiO_2 samples are shown in Figure 3. The TEM images revealed the PPy-TiO_2 composites had a uniform smooth surface and core−shell morphology (Figures 3a and 3b). The outer layer was apparently PPy, and the inner layer was TiO_2 fibers; the thickness of PPy was ~10 nm. Figures 3c and 3d show the TEM images of the PPy-Ag-TiO_2 nanofibers. Compared with PPy-TiO_2 nanofibers, the PPy-Ag-TiO_2 nanofibers were rather uneven. In the two systems, SDS played important role in the formation of PPy-TiO_2 nanofibers. During polymerization, SDS molecules were first absorbed onto the surface of the TiO_2 (or Ag-TiO_2) nanofibers. A columnar micro region containing a hard core (TiO_2 and/or Ag) and a soft interface (SDS) was then formed. After adding the pyrrole monomers and the $FeCl_3$ oxidant, polymerization occurred between the surfactant layer and the Ag or TiO_2 surface. PPy was gradually deposited onto the TiO_2 (or Ag-TiO_2) nanofibers surface, to form PPy-TiO_2 or PPy-Ag-TiO_2 nanofibers.[35,36] The thin layer of PPy on the surface substantially protected the silver from being oxidized.

The UV−vis diffuse reflectance spectra (DRS) of the different samples are illustrated in Figure 4. The pure TiO_2 sample showed the typical absorption of anatase with an intense transition in the UV region of the spectrum, which was due to the promotion of the electron from the valence band to the conduction band. The Ag-TiO_2 sample clearly showed a characteristic absorption of TiO_2 in the UV region and a new absorption shoulder at 400−600 nm that can be attributed to

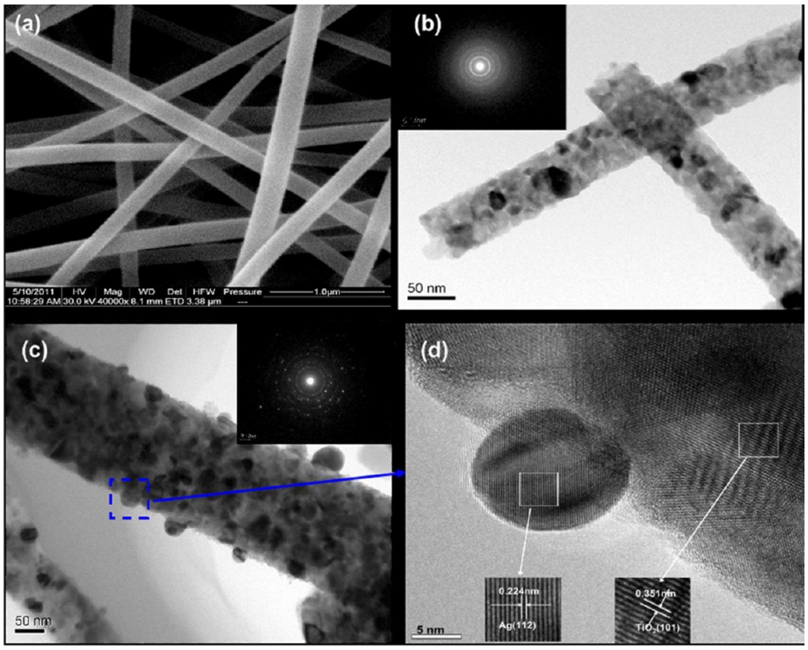

Figure 2. (a) SEM image of TiO_2 nanofibers, (b) TEM image of TiO_2 nanofibers (inset shows the corresponding SAED pattern), (c) TEM image of Ag-TiO_2 nanofibers (inset shows the corresponding SAED pattern), and (d) a high-resolution TEM image of Ag-TiO_2 nanofiber.

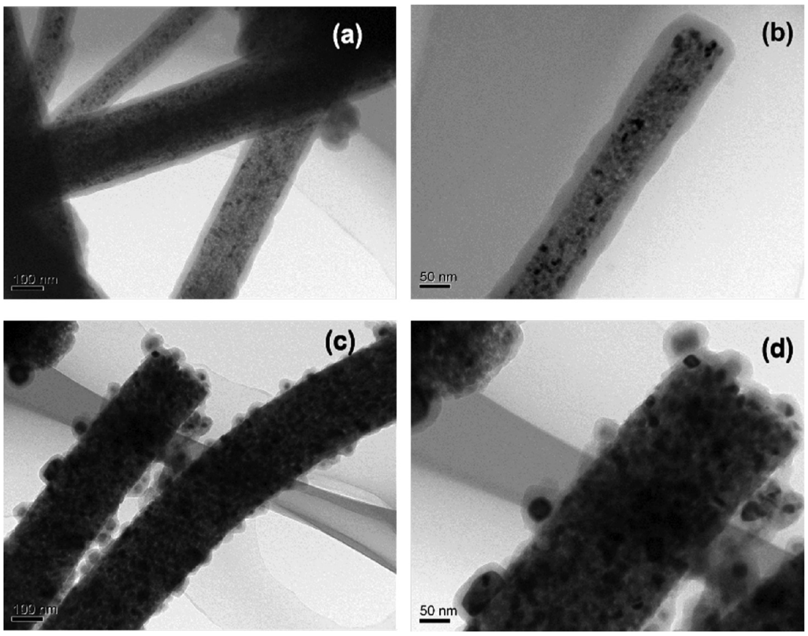

Figure 3. TEM images of (a) PPy-TiO_2 nanofibers, (b) a magnified PPy-TiO_2 nanofiber image, (c) PPy-Ag-TiO_2 nanofibers, and (d) a magnified image of PPy-Ag-TiO_2 nanofiber.

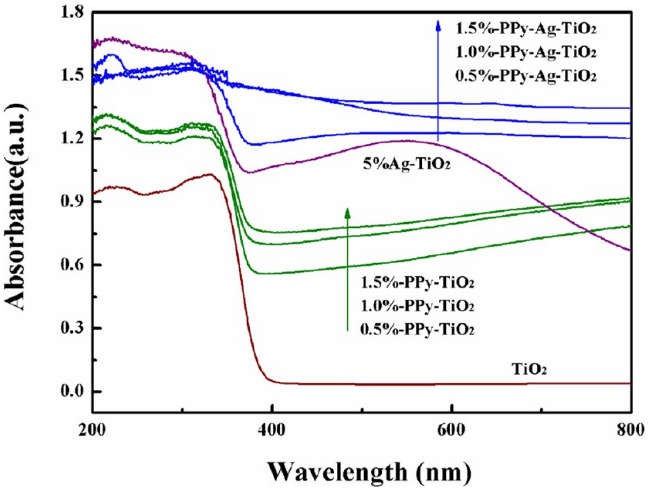

Figure 4. UV−vis absorption spectra of different samples.

the Ag surface plasmon resonance with the TiO_2 interband transition at $\lambda < 380$ nm. Meanwhile, a decrease in the band-gap values can be observed for Ag-TiO_2 photocatalysts, as reported by other authors.[37,38] This decrease was due to the fact that the metallic clusters introduced localized energy levels in the TiO_2 band gap. The electrons can be excited with a lower energy from the valence band (VB) to these levels rather than to the conduction band (CB) of the semiconductor. For the PPy-TiO_2 and PPy-Ag-TiO_2 samples, the introduction of PPy significantly affected the light absorption of TiO_2 and Ag-TiO_2, and the absorption intensity increased with increased PPy doping content, probably because PPy had strong absorption ability within the UV and visible wavelength range. Figure 4 shows that the presence of PPy in the materials is expressed by the continuous band from 400 nm to 800 nm with increased absorption toward the wavelength characteristic of black solids. The adsorption strength of PPy-Ag-TiO_2 was markedly higher than that of PPy-TiO_2, because of the existence of Ag.

The photoluminscence (PL) emission mainly resulted from the recombination of excited electrons and holes, and a lower PL intensity indicated a higher separation efficiency.[39] The PL measurement results for different samples are presented in Figure 5. Figure 5a shows that a strong peak located at ca. 380 nm can be attributed to the recombination of free electrons from the CB bottom to the recombination center at the ground state, because its energy was nearly equal to the band gap (3.20 eV) of TiO_2. The other three peaks observed within the wavelength range of 390−450 nm were attributed to excitonic PL, which mainly resulted from surface oxygen vacancies and defects.[40] Compared with pure TiO_2 sample, the PL intensity of the other three samples significant decreased, indicating that they have lower recombination rate of the photoelectrons carriers than that of pure TiO_2 samples under UV light irradiation. Among these samples, PPy-Ag-TiO_2 had the lowest

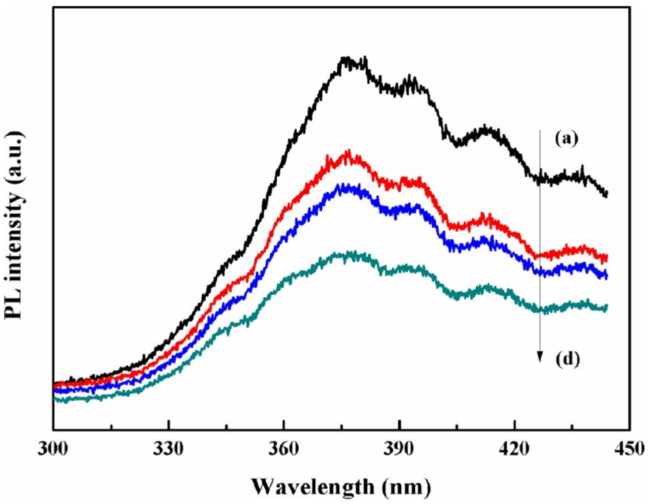

Figure 5. PL emission spectra (excited at 325 nm) of (a) TiO_2, (b) Ag-TiO_2, (c) PPy-TiO_2, and (d) PPy-Ag-TiO_2.

PL intensity, indicating that it had the lowest recombination rate of photoelectrons carriers. This result was due to the fact that the electrons were excited from the valence band to the conduction band and then transferred to the Fermi level of Ag, thereby preventing direct recombination of electrons and holes.

Another methodology was used to detect the transient photocurrent responses to provide further evidence of electron−hole transfer mechanism. Figure 6 shows the typical photocurrent versus time (I−t) response curves for different samples with several on−off cycles of intermittent visible-light irradiation. The initial anodic photocurrent spike caused by the separation of the electron−hole pairs by movement of holes toward the semiconductor surface where they were trapped or reduced by the species in the electrolyte, whereas the electrons were transported to the back contact. After achieving the anodic photocurrent spike, the photocurrent continuously decreased with time until a steady-state photocurrent was reached. The photocurrent decay indicated that charge recombination processes were occurring.[41−44] The photocurrent of the undoped TiO_2, PPy-TiO_2, Ag-TiO_2, and PPy-Ag-TiO_2 electrodes were 0.18, 0.43, 0.54, and 0.83 mA/cm^2, respectively. The photocurrent of the Ag-TiO_2 and PPy-TiO_2 electrodes were ~2.38, which is 3 times higher than those of the TiO_2 electrode, and PPy-Ag-TiO_2 increased the photocurrent further to 4.6 times that of the TiO_2 electrode. The photocurrent followed the order: PPy-Ag-TiO_2 > PPy-TiO_2 > Ag-TiO_2 > pure TiO_2. The obvious enhancement of PPy-Ag-TiO_2 in photocurrent indicated smaller recombination and more efficient separation of photogenerated electron−hole pairs at its interface. The result agreed well with the PL measurement.

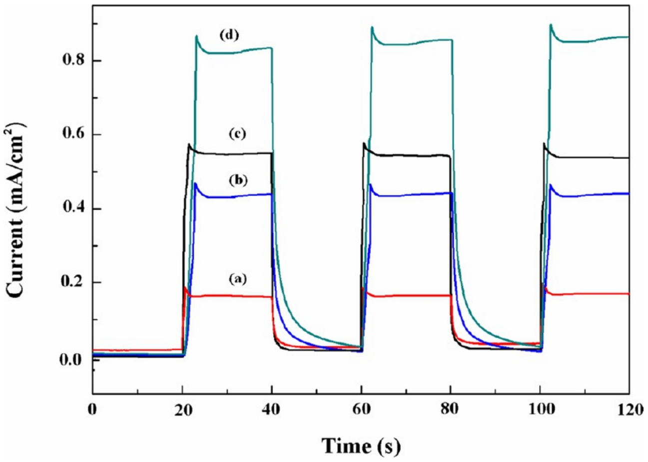

Figure 6. Photocurrent transient responses at a constant potential of 0.5 V for (a) TiO_2, (b) Ag-TiO_2, (c) PPy-TiO_2, and (d) PPy-Ag-TiO_2.

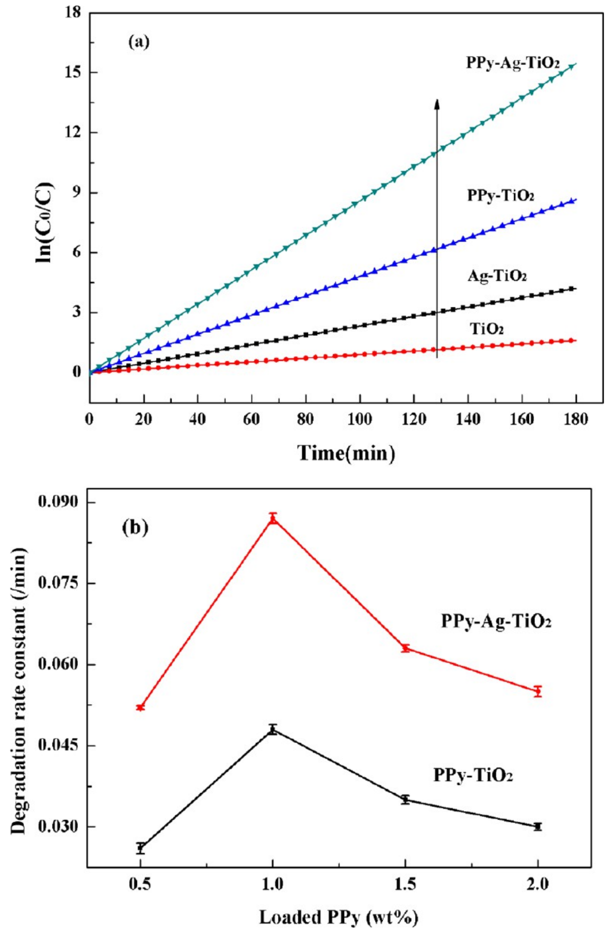

Figure 7. (a) Visible-light-induced photocatalytical activity of different samples. (b) Relationship between photodegradation rate constant and loaded PPy content by PPy-TiO_2 or PPy-Ag-TiO_2.

The photocatalytic activity of different samples was evaluated by measuring the time-dependent degradation of gaseous acetone under visible-light irradiation. The results are shown in Figure 7. It can be seen that the pure TiO_2 nanofiber sample showed poor photocatalytic activities in the visible-light range, the degradation rate constant (k) was ~0.009/min, which was due to the large band-gap energy of TiO_2 (3.0 eV for rutile and 3.2 for anatase). The activity of the Ag-TiO_2 sample was much higher than that of TiO_2, and its rate constant reaches a value of k = 0.023/min. This result may be due to the fact that Ag nanoparticles on the TiO_2 surface can act as a sink for electrons, which contributed to the interfacial charge transfer between the metal and semiconductor and to the separation of photogenerated electron−hole pairs, thereby enhancing the photocatalytic activity. After introducing 1.0 wt % of PPy, the activities of PPy-TiO_2 and PPy-Ag-TiO_2 increased remarkably. The rate constant of PPy-TiO_2 is k = 0.048 min^{-1}, which was 5.33 times that of TiO_2 and 2.07 times that of Ag-TiO_2. PPy-Ag-TiO_2 exhibited much higher photocatalytic activity than the above samples, and its k value was 0.087 min^{-1}, which was 9.66, 3.78, and 1.81 times greater than that of TiO_2, Ag-TiO_2, and PPy-TiO_2, respectively.

The PPy content significantly influenced the photodegradation of gaseous acetone (Figure 7b). The photocatalytic activity of PPy-TiO_2 and PPy-Ag-TiO_2 initially increased and then decreased with increased PPy content from 0.5 wt % to 2.0 wt %. The optimum doping content for PPy was 1.0 wt %, which maybe due to the balance between the increase in highest occupied molecular orbital (HOMO) electrons (PPy) potential and the decrease in light adsorption. High PPy load prevented TiO_2 from absorbing visible light and, consequently, resulted in a rapid decrease of irradiation passing through the reaction system. The higher photocatalytic activity of 1%-PPy-Ag-TiO_2 may be due to the synergistic effect of Ag, PPy, and TiO_2 nanostructures in the ternary system. Kinetics parameters of different samples for degradation of gaseous acetone under visible-light irradiation can be found in Table 1.

A schematic of the charge transfer processes of PPy-Ag-TiO_2 is illustrated in Scheme 1. For PPy-TiO_2, when the PPy shell

Table 1. Kinetics Parameters of Different Samples for Degradation of Gaseous Acetone under Visible-Light Irradiation

photocatalyst	Visible Light	
	K (min^{-1})	R
TiO_2	0.009	0.9958
5% Ag/TiO_2	0.023	0.9903
0.5%-PPy-TiO_2	0.026	0.9943
1.0%-PPy/TiO_2	0.048	0.9970
1.5%-PPy-TiO_2	0.035	0.9920
2.0%-PPy-TiO_2	0.030	0.9926
0.5%-PPy- Ag/TiO_2	0.052	0.9984
1.0%-PPy- Ag/TiO_2	0.087	0.9995
1.5%-PPy- Ag/TiO_2	0.063	0.9964
2.0%-PPy- Ag/TiO_2	0.055	0.9986

Scheme 1. Postulate Mechanism of the Visible Light-Induced Photodegradation of Acetone with PPy-Ag-TiO_2 Nanocomposites

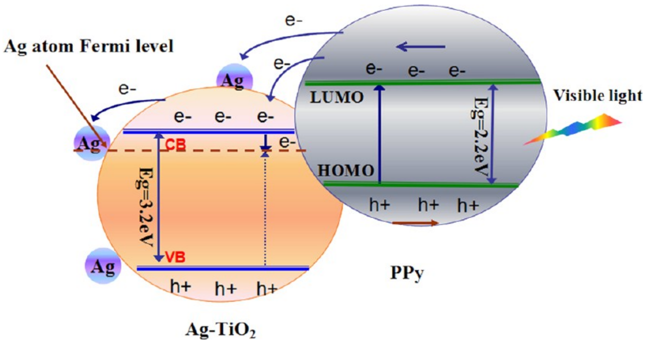

harvested visible light, an absorbed photon promoted an electron from the ground state of the polymer located in the semiconductor energy gap into an excited state that was in resonance with the CB. The polymer π-orbital became the HOMO in the combined system. Given that the lowest unoccupied molecular orbital (LUMO) levels of the polymer were energetically higher than the conduction band edge of TiO_2,[45,46] the electron-transfer paths in Scheme 1 were possible. As a result, rapid charge separation and slow charge recombination occurred, resulting in increased photocatalytic activity.

For PPy-Ag-TiO_2, when the PPy-Ag-TiO_2 composites were illuminated under visible light, their electrons can be excited from the HOMO to the LUMO of PPy, whereas holes were left in the HOMO of PPy. The excited-state electrons can be readily injected into the CB of TiO_2, and then further injected into the Fermi level of Ag, or maybe directly injected into the Fermi level of Ag. The metallic silver nanoparticles functioned as an electron sink to accept the photogenerated electrons from the excited semiconductor, thereby facilitating dioxygen reduction.[47] As a result, PPy-Ag-TiO_2 had a quicker charge separation and slower charge recombination process than PPy-TiO_2 and thus had higher photocatalytic activity. When the addition value of PPy was higher than 1 wt %, the presence of a large amount of PPy can cover the surface of Ag-TiO_2 and form a relatively thick layer that hindered the injection of excited electrons from the outer PPy layer to the inner TiO_2 layer. Consequently, ·OH radicals decreased and the photodecomposition of the target contamination was affected.

Acetone conversion obtained after five successive reaction cycles on 1%-PPy-Ag-TiO_2 samples is shown in Figure 8.

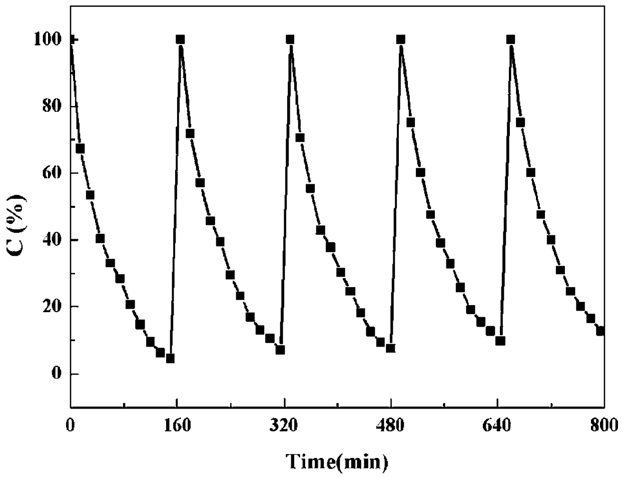

Figure 8. Recycle of PPy-Ag-TiO_2 under visible-light irradiation.

Catalytic recycling studies were carried out by recovering the used catalysts samples after 160 min of reaction and reusing them with fresh reagents in the subsequent reaction cycles, which was repeated five times. The recovered catalysts were washed with acetone/ethanol and dried in air before being reused in the next catalytic test. The results showed that the activity of PPy-Ag-TiO_2 catalysts decreased by ~10% upon five recycling tests. The slight decrease after each cycle was attributed to the absorption of contamination and the decrease in active spots. Although slight decrements in photocatalytic activity were observed, the 1%-PPy-Ag-TiO_2 particles still maintained a high level of activity in successive reusing experiments, indicating that the PPy-Ag-TiO_2 prepared in this study was stable and effective for the removal of organic pollutants.

4. CONCLUSIONS

In summary, PPy-Ag-TiO_2 core/shell nanofibers were successfully prepared through an efficient route. The novel photocatalysts showed obvious visible-light photocatalytic activity in the decomposition gaseous acetone, the 1%-PPy-Ag-TiO_2 sample provided the optimum photocatalytic activity, compared with the pure TiO_2 nanofibers, Ag-TiO_2 nanofibers, and PPy-TiO_2 core−shell nanofibers under visible-light irradiation. The high photoactivity of the PPy-Ag-TiO_2 can be attributed to the synergistic effect originating from the excited-state electrons in PPy can be readily injected into the TiO_2 CB and be further injected into the Fermi level of Ag. As a result, rapid charge separation and slow charge recombination occurred, resulting in increased photocatalytic activity. The recycling test revealed that the PPy-Ag-TiO_2 prepared in this study was stable and effective for the removal of organic pollutants. Therefore, the method described in this paper provided a simple and effective strategy for the rational design of delicate composite photocatalysts for applications beyond photocatalysis.

■ ASSOCIATED CONTENT

Ⓢ Supporting Information

The photograph and schematic of the basic experimental setup for electrospinning, FT-IR spectra of different samples, the diagram of Ag particle size distribution, photocurrent transient responses, and UV−vis spectra of PPy can be found in the Supporting Information. This material is available free of charge via the Internet at http://pubs.acs.org.

AUTHOR INFORMATION

Corresponding Author

*E-mails: jhwei@whu.edu.cn (J.H.W.), cxpan@whu.edu.cn (C.X.P.).

Notes

The authors declare no competing financial interest.

ACKNOWLEDGMENTS

We are grateful for the financial support from the National Natural Science Foundation of China (No. 51272185) and the National Program on Key Basic Research Project (973 Grant Nos. 2009CB939705 and 2012CB821404).

REFERENCES

(1) Iijima, S. *Nature* **1991**, *354*, 56−58.
(2) Tong, H.; Ouyang, S. X.; Bi, Y. P.; Umezawa, N.; Oshikiri, M.; Ye, J. H. *Adv. Mater.* **2012**, *24*, 229−251.
(3) Zhou, W. J.; Du, G. J.; Hu, P . G.; Wang, D. Z.; Liu, H.; Wang, J. Y.; Boughton, R. I.; Liu, D.; Jiang, H. D. *J. Mater. Chem.* **2011**, *21*, 7937−7945.
(4) Choi, S. K.; Kim, S.; Lim, S. K.; Park, H. *J. Phys. Chem. C* **2010**, *114*, 16475−16480.
(5) Shah, M. S. A. S.; Park, A. R.; Zhang, K.; Park, J. H.; Yoo, P. J. *ACS Appl. Mater. Interfaces* **2012**, *4*, 3893−3901.
(6) Yang, L.; Xiao, Y.; Liu, S.; Li, Y.; Cai, Q.; Luo, S.; Zeng, G. *Appl. Catal., B* **2010**, *94*, 142−149.
(7) Tang, Y.; Luo, S.; Teng, Y.; Liu, C.; Xu, X.; Zhang, X.; Chen, L. *J. Hazard. Mater.* **2012**, *241- 242*, 323−330.
(8) Yang, L.; Chen, B.; Luo, S.; Li, J.; Liu, R.; Cai, Q. *Environ. Sci. Technol.* **2010**, *44*, 7884−7889.
(9) Yang, L.; Luo, S.; Li, Y.; Xiao, Y.; Kang, Q.; Cai, Q. *Environ. Sci. Technol.* **2010**, *44*, 7641−7646.
(10) Livraghi, S.; Paganini, M. C.; Giamello, E.; Selloni, A.; Valentin, C. D.; Pacchioni, G. *J. Am. Chem. Soc.* **2006**, *128*, 15666−15671.
(11) Mohamed, A. E. R.; Rohani, S. *Energy Environ. Sci.* **2011**, *4*, 1065−1086.
(12) Lee, S. S.; Fan, C. Y.; Wu, T. P.; Anderson, S. L. *J. Am. Chem. Soc.* **2004**, *126*, 5682−5683.
(13) Zhang, L. W.; Fu, H. B.; Zhu, Y. F. *Adv. Funct. Mater.* **2008**, *18*, 2180−2189.
(14) Cheng, H.; Zhao, X. J.; Sui, X. T.; Xiong, Y. L.; Zhao, J. *J. Nanopart. Res.* **2011**, *13*, 555−562.
(15) Chuang, H. Y.; Chen, D. H. *Nanotechnology* **2009**, *20*, 105704/1−105704/10.
(16) Kandiel, T. A.; Dillert, R.; Bahnemann, D. W. *Photochem. Photobiol. Sci.* **2009**, *8*, 683−690.
(17) Chen, A. H.; Xie, H. X.; Wang, H. Q.; Li, H. Y.; Li, X. Y. *Synth. Met.* **2006**, *156*, 346−350.
(18) Chowdhury, D.; Paul, A.; Chattopadhyay, A. *Langmuir* **2005**, *21*, 4123−4128.
(19) Xu, S. B.; Zhu, Y. F.; Jiang, L.; Dan, Y. *Water, Air, Soil Pollut.* **2010**, *213*, 151−159.
(20) Li, X. Y.; Wang, D. S.; Cheng, G. X.; Luo, Q. Z.; An, J.; Wang, Y. H. *Appl. Catal., B* **2008**, *81*, 267−273.
(21) Li, S. Y.; Chen, M. K.; He, L. J.; Xu, F.; Zhao, G. H. *J. Mater. Res.* **2009**, *24*, 2547−2554.
(22) Huang, K.; Wan, M. X.; Long, Y. Z.; Chen, Z. J.; Wei, Y. *Synth. Met.* **2005**, *155*, 495−500.
(23) Wei, J. H.; Zhang, Q.; Liu, Y.; Xiong, R.; Pan, C. X.; Shi, J. *J. Nanopart. Res.* **2011**, *13*, 3157−3165.
(24) Frank, A. J.; Honda, K. *J. Photochem.* **1985**, *29*, 195−204.
(25) Wang, J.; Ni, X. Y. *Solid State Commun.* **2008**, *146*, 239−244.
(26) Kamat, P. V. *J. Phys. Chem. Lett.* **2012**, *3*, 663−672.
(27) Kamat, P. V. *J. Phys. Chem. B* **2002**, *106*, 7729−7744.
(28) Zhang, P.; Shao, C. L.; Zhang, Z. Y.; Zhang, M. Y.; Mu, J. B.; Guo, Z. C.; Sun, Y. Y.; Liu, Y. C. *J. Mater. Chem.* **2011**, *21*, 17746−17753.
(29) Chuangchote, S.; Jitputti, J.; Sagawa, T.; Yoshikawa, S. *ACS Appl. Mater. Interfaces* **2009**, *1*, 1140−1143.
(30) Lu, X. F.; Mao, H.; Zhang, W. J. *Nanotechnology* **2007**, *18*, 025604/1−025604/5.
(31) Choi, S. K.; Kim, S.; Lim, S. K.; Park, H. *J. Phys. Chem. C* **2010**, *114*, 16475−16480.
(32) Su, P. G.; Chang, Y. P. *Sens. Actuators, B* **2008**, *129*, 915−920.
(33) Ochandaw, F. O.; Barnett, M. R. *J. Am. Ceram. Soc.* **2010**, *93*, 2637−2643.
(34) Wang, B.; Li, C.; Pang, J. F.; Qing, X. T.; Zhai, J. P.; Li, Q. *Appl. Surf. Sci.* **2012**, *258*, 9989−9996.
(35) Pinter, E.; Patakfalvi, R.; Fullei, T.; Ging, Z.; Dekany, I.; Visy, C. *J. Phys. Chem. B* **2005**, *109*, 17474−17478.
(36) Ye, S.; Fang, L.; Lu, Y. *Phys. Chem. Chem. Phys.* **2009**, *11*, 2480−2484.
(37) Hu, C.; Lan, Y. Q.; Qu, J. H.; Hu, X. X.; Wang, A. M. *J. Phys. Chem. B* **2006**, *110*, 4066 −4072.
(38) Melian, E. P.; Diaz, O. G.; Rodriguez, J. M. D.; Colon, G.; Navio, J. A.; Macias, M.; Pena, J. P. *Appl. Catal., B* **2012**, *127*, 112−120.
(39) Ishibashi, K.; Fujishima, A.; Watanabe, T.; Hashimoto, K. *Electrochem. Commun.* **2000**, *2*, 207−210.
(40) Yu, J. G.; Xiang, Q. J.; Zhou, M. H. *Appl. Catal., B* **2009**, *90*, 595−602.
(41) Spadavecchia, F.; Ardizzone, S.; Cappelletti, G.; Falciola, L.; Ceotto, M.; Lotti, D. *J. Appl. Electrochem.* **2013**, *43*, 217−225.
(42) Dholam, R.; Patel, N.; Santini, A.; Miotello, A. *Int. J. Hydrogen Energy* **2010**, *35*, 9581−9590.
(43) Hagfeldt, A.; Lindstrom, H.; Sodergren, S.; Lindquist, S. E. *J. Electroanal. Chem.* **1995**, *381*, 39−46.
(44) Sakai, N.; Ebina, Y.; Takada, K.; Sasaki, T. *J. Am. Chem. Soc.* **2004**, *126*, 5851−5858.
(45) Wang, D. S.; Wang, Y. H.; Li, X. Y.; Luo, Q. Z.; An, J.; Yue, J. X. *Catal. Commun.* **2008**, *9*, 1162−1166.
(46) Murakoshi, K.; Kogure, R.; Wada, Y.; Yanagida, S. *Chem. Lett.* **1997**, *26*, 471−472.
(47) Liu, R.; Wang, P.; Wang, X. F.; Yu, H. G.; Yu, J. G. *J. Phys. Chem. C* **2012**, *116*, 17721−17728.